Monthly Notices
of the
ROYAL ASTRONOMICAL SOCIETY

Mon. Not. R. Astron. Soc. **420,** 2978–2989 (2012) doi:10.1111/j.1365-2966.2011.20149.x

Statistics of substructures in dark matter haloes

E. Contini,[1,2]★ G. De Lucia[2] and S. Borgani[1,2,3]

[1]*Dipartimento di Astronomia, Universitá di Trieste, via G.B. Tiepolo 11, I-34131 Trieste, Italy*
[2]*INAF – Astronomical Observatory of Trieste, via G.B. Tiepolo 11, I-34143 Trieste, Italy*
[3]*INFN, Sezione di Trieste, Via Valerio 2, I-34127 Trieste, Italy*

Accepted 2011 November 7. Received 2011 October 11; in original form 2011 August 8

ABSTRACT

We study the amount and distribution of dark matter substructures within dark matter haloes, using a large set of high-resolution simulations ranging from group-size to cluster-size haloes, and carried out within a cosmological model consistent with *Wilkinson Microwave Anisotropy Probe* (*WMAP*) 7-year data. In particular, we study how the measured properties of subhaloes vary as a function of the parent halo mass, the physical properties of the parent halo and redshift. The fraction of halo mass in substructures increases with increasing mass: it is of the order of 5 per cent for haloes with $M_{200} \sim 10^{13}\,\mathrm{M}_{\odot}$ and of the order of 10 per cent for the most massive haloes in our sample, with $M_{200} \sim 10^{15}\,\mathrm{M}_{\odot}$. There is, however, a very large halo-to-halo scatter that can be explained only in part by a range of halo physical properties, e.g. concentration. At a given halo mass, less concentrated haloes contain significantly larger fractions of mass in substructures because of the reduced strength of tidal disruption. Most of the substructure mass is located at the outskirts of the parent haloes, in relatively few massive subhaloes. This mass segregation appears to become stronger at increasing redshift, and should reflect into a more significant mass segregation of the galaxy population at different cosmic epochs. When haloes are accreted on to larger structures, their mass is significantly reduced by tidal stripping. Haloes that are more massive at the time of accretion (these should host more luminous galaxies) are brought closer to the centre on shorter time-scales by dynamical friction, and therefore suffer a more significant stripping. The halo merger rate depends strongly on the environment with substructure in more massive haloes suffering more important mergers than their counterparts residing in less massive systems. This should translate into a different morphological mix for haloes of different mass.

Key words: Galaxy: formation – galaxies: clusters: general – galaxies: evolution – dark matter.

1 INTRODUCTION

In the currently accepted Λ cold dark matter (ΛCDM) paradigm for cosmic structure formation, small dark matter (DM) haloes form first while more massive haloes form later through accretion of diffuse matter and mergers between smaller systems. During the last decades, we have witnessed a rapid development of numerical algorithms and a significant increase in numerical resolution, which have allowed us to improve our knowledge of the formation and evolution of DM structures. In particular, the increase in numerical resolution has allowed us to overcome the so-called *overmerging problem*, i.e. the rapid disruption of galaxy-size substructures in groups and clusters (see Klypin et al. 1999, and references therein). If any, we are now facing the opposite problem, at least on galaxy scales, where many more substructures than visible dwarf galaxies are found (see Ishiyama, Fukushige & Makino 2009; Tikhonov & Klypin 2009, and references therein).

According to the two-stage theory proposed by White & Rees (1978), the physical properties of galaxies are determined by cooling and condensation of gas within the potential wells of DM haloes. Therefore, substructures represent the birth sites of luminous galaxies, and the analysis of their mass and spatial distribution as well as of their merger histories and mass accretion histories (MAHs) provide important information about the expected properties of galaxies in the framework of hierarchical galaxy formation models.

Nowadays, a wealth of substructures is routinely identified in dissipationless simulations, and their statistical properties and evolution have been studied in detail in the past years. The identification of DM substructures, or *subhaloes*, remains a difficult technical task that can be achieved using different algorithms (see e.g. Knebe et al. 2011). Each of these has its own advantages and weaknesses, and different criteria for defining the boundaries and membership of substructures are likely leading to systematic differences between

★E-mail: contini@oats.inaf.it

the physical properties of subhaloes identified through different algorithms. However, these might be probably corrected using simple scaling factors, as suggested by the fact that different studies find very similar slopes for the subhalo mass function, i.e. the distribution of substructures as a function of their mass. This is one of the most accurately studied properties of DM substructures, although it remains unclear if and how it depends on the parent halo mass. Moore et al. (1999) used one high-resolution simulation of a cluster-size halo and one high-resolution simulation of a galaxy-size halo, and found that the latter can be viewed as a scaled version of the former. Later work done by De Lucia et al. (2004) used larger samples of simulated haloes, but found no clear variation of the subhalo mass function as a function of the parent halo mass. Such a dependency was later found by Gao et al. (2004b) and Gao et al. (2011), who showed that the subhalo mass function varies systematically as a function of halo mass and halo physical properties like concentration and formation time.

Typically, only about 10 per cent of the total mass of a DM halo is found in substructures. In addition, their spatial distribution is found to be *antibiased* with respect to that of DM (Ghigna et al. 2000; De Lucia et al. 2004; Nagai & Kravtsov 2005; Saro et al. 2010). It is unclear if the radial distribution of substructures depends on the parent halo mass. De Lucia et al. (2004) found hints for a steeper radial number density profiles of substructures in low-mass haloes than in high-mass haloes. They used, however, a relatively small sample of simulated haloes that were run with different codes and numerical parameters. In this study, we will re-address this issue by using a much larger sample of simulated haloes, all run with the same code and numerical parameters.

Most previous work focusing on DM substructures have studied their properties as a function of their *present-day* mass. This quantity cannot be, however, simply related to the luminosity of the galaxies residing in the substructures under consideration. Indeed, DM substructures are very fragile systems that are strongly affected by tidal stripping (De Lucia et al. 2004; Gao et al. 2004b). Since this process affects primarily the outer regions of subhaloes, and galaxies reside in their inner regions, it is to be expected that the galaxy luminosity/stellar mass is more strongly related to the mass of the substructure at the time of *infall* (i.e. before becoming a substructure) than at present (Gao et al. 2004a; Vale & Ostriker 2006; Wang et al. 2006). In this paper, we will study the evolution of DM substructures splitting our samples according to different values of the mass at infall.

In this paper, we take advantage of a large set of N-body simulations covering a wide dynamical range in halo mass, and with relatively high resolution. This will allow us to study how the statistical properties of substructures vary as a function of halo mass, cosmic epoch and physical properties of the parent halo. The paper is organized as follows. In Section 2, we introduce the simulation set and samples used in our study. In Section 3, we study how the subhalo mass function and subhalo spatial distribution vary as a function of halo mass, redshift and concentration. In the second part of our paper (Section 4), we discuss the mass accretion and merging histories of subhaloes as a function of their mass, accretion time and environment. Finally, in Section 5, we discuss our findings and give our conclusions.

2 CLUSTER SIMULATIONS

Our set of DM haloes is based on 'zoom-in' simulations of 27 Lagrangian regions extracted around massive DM haloes, originally identified within a low-resolution N-body cosmological simulation. For a detailed discussion of this simulation set, we refer to Bonafede et al. (2011, see also Fabjan et al. 2011). The parent simulation followed 1024^3 DM particles within a box of $1\,h^{-1}$ Gpc comoving on a side. The adopted cosmological model assumed $\Omega_{\rm m} = 0.24$ for the matter density parameter, $\Omega_{\rm bar} = 0.04$ for the contribution of baryons, $H_0 = 72\,{\rm km\,s^{-1}\,Mpc^{-1}}$ for the present-day Hubble constant, $n_{\rm s} = 0.96$ for the primordial spectral index, and $\sigma_8 = 0.8$ for the normalization of the power spectrum. The latter is expressed as the rms fluctuation level at $z = 0$ within a top-hat sphere of $8\,h^{-1}$ Mpc radius. With this parameter choice, the assumed cosmogony is consistent with constraints derived from 7-year data from the *Wilkinson Microwave Anisotropy Probe* (*WMAP*7; Komatsu et al. 2011).

Table 1. Our simulation set has been split in five subsamples, according to the halo mass. In the first column, we give the name of the subsample, while the second column gives the range of M_{200} values corresponding to each subsample. The third and fourth columns give the number of haloes and mean number of subhaloes (with mass above $2 \times 10^9\,h^{-1}\,{\rm M}_\odot$) within the virial radius (R_{200}), respectively.

Name	Mass range	$N_{\rm haloes}$	$\bar{N}_{\rm subs}$
S1	$\geq 10^{15}\,h^{-1}\,{\rm M}_\odot$	13	2943
S2	$(5\text{–}10) \times 10^{14}\,h^{-1}\,{\rm M}_\odot$	15	1693
S3	$(1\text{–}5) \times 10^{14}\,h^{-1}\,{\rm M}_\odot$	25	358
S4	$(5\text{–}10) \times 10^{13}\,h^{-1}\,{\rm M}_\odot$	29	146
S5	$(1\text{–}5) \times 10^{13}\,h^{-1}\,{\rm M}_\odot$	259	40

The selected Lagrangian regions were chosen so that 13 of them are centred around the 13 most massive clusters found in the cosmological volume, all having virial[1] mass $M_{200} \simeq 10^{15}\,h^{-1}\,{\rm M}_\odot$. Additional regions were chosen around clusters in the mass range $M_{200} \simeq (5\text{–}10) \times 10^{14}\,h^{-1}\,{\rm M}_\odot$. Within each Lagrangian region, we increased mass resolution and added the relevant high-frequency modes of the power spectrum, using the zoomed initial condition (ZIC) technique presented by Tormen, Bouchet & White (1997). Outside the regions of high resolution, particles of mass increasing with distance are used, so that the computational effort is concentrated on the cluster of interest, while a correct description of the large-scale tidal field is preserved. For the simulations used in this study, the initial conditions have been generated using $m_{\rm DM} = 10^8\,h^{-1}\,{\rm M}_\odot$ for DM particle mass in the high-resolution regions. This mass resolution is a factor 10 better than the value used by Bonafede et al. (2011) and Fabjan et al. (2011) to carry out hydrodynamic simulations for the same set of haloes.

Using an iterative procedure, we have shaped each high-resolution Lagrangian region so that no low-resolution particle 'contaminates' the central 'zoomed-in' halo, out to five virial radii of the main cluster at $z = 0$. In our simulations, each high-resolution region is sufficiently large to contain more than one interesting massive halo, with no 'contaminants', out to at least one virial radius. Our final sample contains 341 haloes with mass larger than $10^{13}h^{-1}\,{\rm M}_\odot$. We have split this sample into five different subsamples, as indicated in Table 1, where we list the number of non-contaminated haloes for each sample and the mean number of substructures per halo in each subsample.

[1] Here we define the virial mass (M_{200}) as the mass contained within the radius R_{200}, which encloses a mean density of 200 times the critical density of the Universe at the redshift of interest.

Simulations have been carried out using the Tree-PM GADGET-3 code. We adopted a Plummer-equivalent softening length for the computation of the gravitational force in the high-resolution region. This is fixed to $\epsilon = 2.3\,h^{-1}$ kpc in physical units at redshift $z < 2$, and in comoving units at higher redshift. For each simulation, data have been stored at 93 output times between $z \sim 60$ and $z = 0$. DM haloes have been identified using a standard friends-of-friends (FOF) algorithm, with a linking length of 0.16 in units of the mean interparticle separation in the high-resolution region. The algorithm SUBFIND (Springel, Yoshida & White 2001) has then been used to decompose each FOF group into a set of disjoint substructures, identified as locally overdense regions in the density field of the background halo. As in previous work, only substructures which retain at least 20 bound particles after a gravitational unbinding procedure are considered to be genuine substructures. Given our numerical resolution, the smallest structure we can resolve has a mass of $M = 2 \times 10^9\,h^{-1}\,\mathrm{M}_\odot$. To avoid being too close to the resolution limit of the simulations, we will sometimes consider only substructures that contain at least 100 particles, i.e. we will adopt a mass limit of $1 \times 10^{10}\,h^{-1}\,\mathrm{M}_\odot$.

3 AMOUNT AND DISTRIBUTIONS OF DARK MATTER SUBSTRUCTURES

In this section we will consider some basic statistics of the DM substructures in our sample. In particular, we will address the following questions: what is the mass fraction in substructures? What is their mass and spatial distribution? And how do these properties vary as a function of the halo mass, or as a function of other physical properties of the parent haloes? As discussed above, if subhaloes are to be considered the places where galaxies are located, these statistics provide us important information about the statistical properties of cluster galaxy populations expected in hierarchical cosmologies.

3.1 Mass fraction in subhaloes

Previous work has found that only 5–10 per cent of the halo mass is contained in substructures, with most of it actually contained in relatively few massive subhaloes (Ghigna et al. 1998, 2000; Springel et al. 2001; Stoehr et al. 2003; De Lucia et al. 2004; Gao et al. 2004b).

Results for our simulation set are shown in Fig. 1. The top-left panel shows the cumulative mass fraction in subhaloes above the mass indicated on the x-axis, for the five samples considered in our study. There is a clear trend for an increasing mass in substructures for more massive haloes. For our most massive sample (S1), about 10 per cent of the halo mass is contained in substructures more massive than $2 \times 10^9\,h^{-1}\,\mathrm{M}_\odot$, and approximately 10 per cent of the mass in substructures is contained in the most massive ones. For less massive haloes, the mass fraction in substructures decreases.

Most of the substructures are located outside the central core of DM haloes. In particular, the top-right panel of Fig. 1 shows that the substructure mass fraction is smaller than $\sim$1 per cent out to $\sim 0.3 \times r_{200}$, and increases to half its total (within r_{200}) value at $\sim 0.8 \times r_{200}$. The results shown can be explained by considering that haloes of larger mass are less concentrated and dynamically younger than their less massive counterparts. As we will show below, and as discussed in previous studies, subhaloes are strongly affected by dynamical friction and tidal stripping. Less massive haloes assemble earlier than their more massive counterparts, i.e. accrete most of the haloes that contribute to their final mass at early times, so that there was enough time to 'erase' the structures below the resolution of the simulation in these systems. In addition, haloes that were accreted earlier, and therefore suffered tidal stripping for longer times, are preferentially located closer to the centre (see fig. 15 in Gao et al. 2004b).

For haloes of the same mass, a relatively large range of concentrations is possible so that a range of mass fractions is expected. This is confirmed in the bottom panels of Fig. 1 where we have considered only haloes in our least massive sample (S5), and split it into three different bins according to the halo concentration so as to have the same number of haloes for each bin. We approximate the concentration by $V_{\rm max}/V_{200}$, where $V_{\rm max}$ is the maximum circular velocity, which is computed by considering all particles bound to a given halo, while $V_{200} = \sqrt{GM_{200}/R_{200}}$. Interestingly, the lowest concentration bin contains substructure mass fractions that are, on average, very close to those of our most massive samples (S1 in the top panels). This confirms that the halo-to-halo scatter is very large, and that it can be explained only in part by haloes in the same mass bin covering a range of physical properties. In order to give an idea of the intrinsic scatter of haloes in the same mass bin, we have repeated the last point in the top-right panel of Fig. 1, showing this time the median and the 25th and 75th percentile of the distributions obtained at $R/R_{200} = 1$.

3.2 Subhalo mass function

One of the most basic statistics of the subhalo population is provided by the subhalo mass function, i.e. the distribution of DM substructures as a function of their mass. This has been analysed in many previous studies with the aim to answer the following questions: does the subhalo mass function vary as a function of the parent halo mass? How does it vary as a function of cosmic time? How does it vary as a function of halo properties (e.g. concentration, formation time, etc.)?

First studies were based on very small samples of simulated haloes, and claimed the 'universality' of the subhalo mass function. For example, Moore et al. (1999) compared the substructure mass distribution obtained for one simulated cluster of mass similar to that of the Virgo cluster, and one simulated galaxy-size halo, and argued that galactic haloes can be considered as 'scaled versions' of cluster-size haloes. De Lucia et al. (2004) used a sample of $\sim$11 high-resolution resimulations of galaxy clusters together with a simulation of a region with average density. They argued that the subhalo mass function depends *at most weakly* on the parent halo mass, and that the (nearly) invariance of the subhalo mass function could lie in the physical nature of the dynamical balance between two opposite effects: the destruction of substructures due to dynamical friction and tidal stripping on the one hand, and the accretion of new substructures on the other hand. Contemporary work by Gao et al. (2004b) and later work (e.g. Gao et al. 2011) have demonstrated that the subhalo mass function does depend on the parent halo mass, as well as on the physical properties of the parent halo, in particular its concentration and formation time. We note that Gao et al. (2004b) used a sample of simulated haloes that was not homogeneous in terms of resolution (typically lower than ours), cosmological parameters and simulation codes. The sample used in Gao et al. (2011) was instead based on a homogeneous set of cosmological parameters (consistent with *WMAP* 1-year results) and included simulations with resolution higher than that of our sample. Their sample, however, did not include very massive haloes ($\sim 10^{15}\,h^{-1}\,\mathrm{M}_\odot$). It is therefore interesting to re-address the questions listed above using our simulation sample.

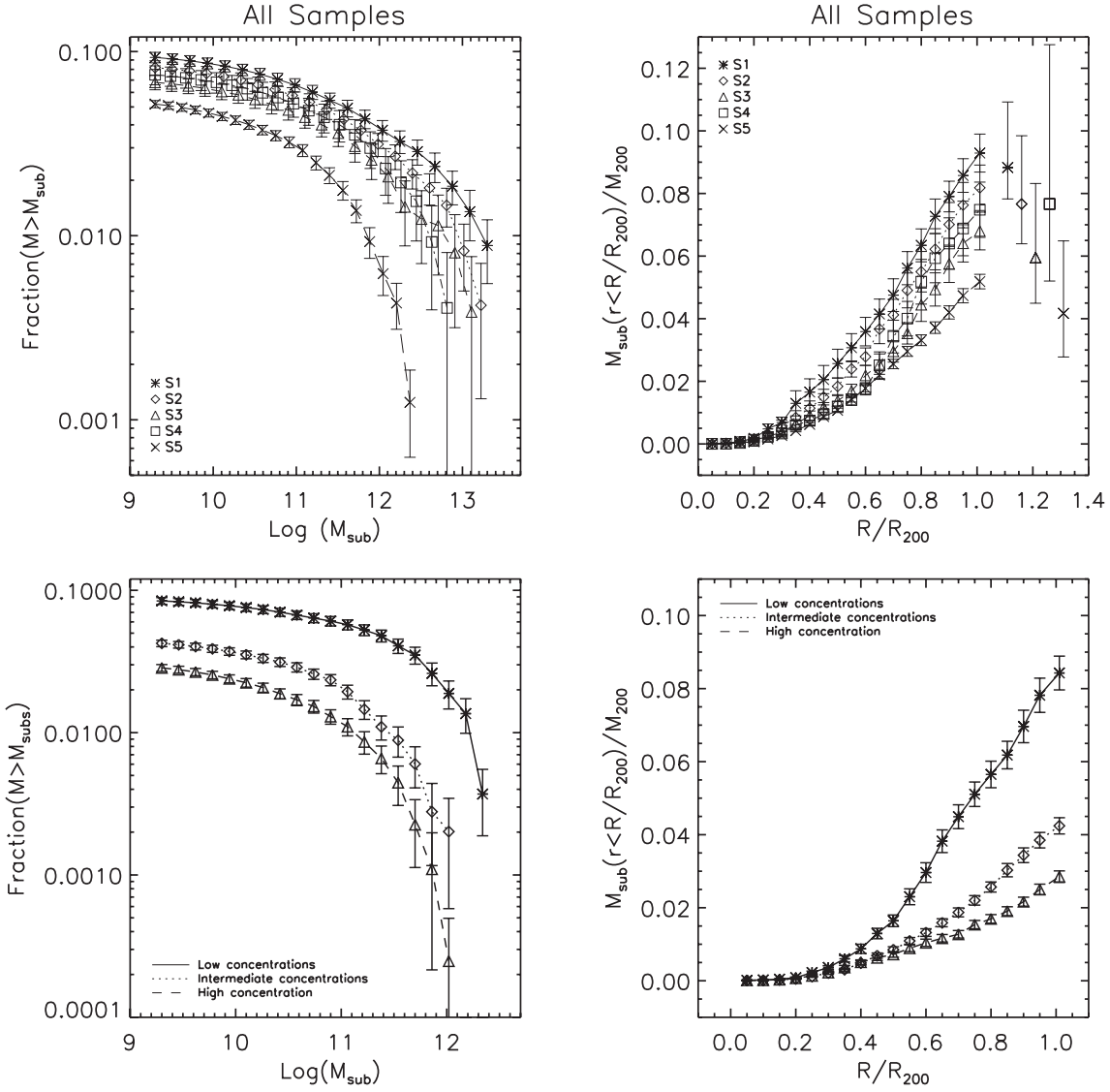

Figure 1. Top panels: cumulative mass fraction in substructures as a function of subhalo mass (left) and normalized distance from the halo centre (right), for the five samples used in this study (different symbols, as indicated in the legend). In the right-hand panel the rightmost symbols with error bars show the median, 25th and 75th percentile of the distributions at $R/R_{200} = 1$. Bottom panels: same as in the top panels but using only haloes from our sample S5 (the least massive one), and splitting the sample in three different bins according to the concentration of the parent haloes. In all panels, symbols connected by lines show the mean values, while error bars show the rms scatter around the mean.

In Fig. 2, we plot the slope of the differential mass function obtained by fitting a power law to the mass functions of each subsample considered in our study. Following De Lucia et al. (2004), we have restricted the fit by discarding the most massive (and rarest) substructures (those with mass above $10^{12}\,h^{-1}\,\mathrm{M}_{\odot}$ for the samples S1 and S2, and with mass above $10^{11.5}\,h^{-1}\,\mathrm{M}_{\odot}$ for the samples S3, S4 and S5). We find that, albeit weakly, the slope of the subhalo mass function depends on the parent halo mass, and that there is a weak trend for shallower slopes with increasing look-back times. The best-fitting values we measure vary in the range between ~ -0.65 and -0.8, in agreement with results from previous studies (e.g. Ghigna et al. 2000; De Lucia et al. 2004; Gao et al. 2004b). When including the most massive substructures in the fit, we obtain steeper slopes, ranging from ~ -0.91 to -0.86 at redshift $z = 0$, but the trends shown in Fig. 2 are not altered significantly.

As explained by Gao et al. (2011), the dependence of the subhalo mass function on halo mass is a consequence of the fact that more massive haloes are on average less concentrated and dynamically younger than their less massive counterparts. Since the strength of tidal disruption depends on halo concentration, and since haloes of a given mass are on average less concentrated at higher redshift, we also expect that the subhalo mass function depends on time. Fig. 3 shows the cumulative subhalo mass function (normalized as in Gao et al. 2004b) at four different redshifts in the left-hand panels and for different concentrations in the right-hand panels (in these panels, only haloes identified at redshift zero have been considered). Top and bottom panels refer to the haloes in the mass range (1–3) $\times\ 10^{13}$ and (1–5) $\times\ 10^{14}\,h^{-1}\,\mathrm{M}_{\odot}$, respectively. We derive the three subsamples by splitting the range of concentration in order to have the same number of haloes in each subsample. Results shown in Fig. 3 confirm previous findings by Gao et al. (2011), and extend them to larger parent halo masses: haloes at higher redshift have significantly more substructures than those of the same mass at later times. The figure suggests that there is a

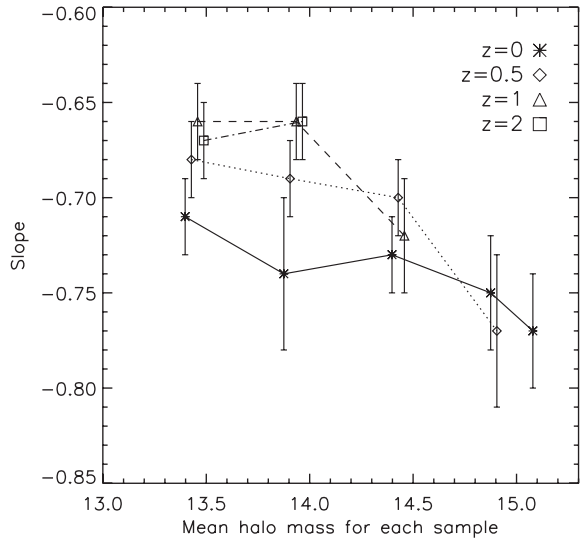

Figure 2. Slope of the differential mass function measured for the different samples considered in this study, at different cosmic epochs (solid line for $z = 0$, dotted for $z = 0.5$, dashed line for $z = 1$ and dot–dashed line for $z = 2$). Error bars are computed as the standard deviation of the slopes measured for each halo within the sample. For reasons of clarity, a small shift has been added to the abscissa.

significant evolution between $z = 0$ and $z \sim 0.5$, but it becomes weaker at higher redshifts. We note that for the highest redshift considered, the subhalo mass function does not significantly differ from that found at $z \sim 1$, but we note that this could be due to poor statistics. Gao et al. (2011) find a similar trend for haloes of similar mass. At any given cosmic epoch, there is a large halo-to-halo scatter which is due, at least in part, to internal properties of the parent halo like concentration, as shown in the right-hand panels of Fig. 3. For the ranges of mass shown in Fig. 3, low-concentration haloes host up to an order of magnitude more substructures than haloes of the same mass but with higher concentration. The differences between the different concentration bins are larger (and significant) for the most massive substructures.

In order to verify that the results of our analysis are robust against numerical resolution, we have compared the cumulative subhalo mass function obtained for the set of simulated haloes presented here to that obtained for the same haloes simulated at a 10 times lower mass resolution. We find that the two distributions agree very well to each other, within the mass range accessible to both resolutions. This confirms that both our simulations and the procedure of halo identification are numerically converged.

3.3 Radial distribution of subhaloes

Previous studies (Ghigna et al. 2000; De Lucia et al. 2004; Nagai & Kravtsov 2005; Saro et al. 2010) have shown that subhaloes are 'antibiased' relative to the DM in the inner regions of haloes. No significant trend has been found as a function of the parent halo mass, with only hints for a steeper profiles of subhaloes in less massive haloes (De Lucia et al. 2004).

The analysis of our sample of simulated haloes confirms previous findings that DM subhaloes are antibiased with respect to DM, with no dependence on parent halo mass. In fact, there is no physical reason to expect such a trend. We note that De Lucia et al. (2004), who found hints for such a correlation, used a smaller sample of simulated haloes that were carried out using different simulation codes and parameters. In contrast, our simulated haloes are all carried out using the same parameters and simulation code.

Nagai & Kravtsov (2005) find that the antibias is much weaker if subhaloes are selected on the basis of the mass they had at the time of accretion on to their parent halo. We confirm their results in Fig. 4, where we show the radial distribution of substructures in our sample S1 (the most massive haloes in our simulation set). The top panel of Fig. 4 shows the radial distribution of substructures selected on the basis of their present-day mass, while in the middle panel the mass of the substructure at the time of accretion (defined as the last time the halo was identified as a central halo, see below) has been used. The figure shows that, in this case, selecting progressively more massive substructures reduces the antibias between subhaloes and DM. The bottom panel of Fig. 4 shows that the same is obtained by discarding substructures that are accreted recently. The two selections tend to pick up haloes that suffered a stronger dynamical friction (i.e. haloes that were more massive at the time of accretion) or that suffered dynamical friction for a longer time (haloes that were accreted earlier). As a consequence, both selections tend to preferentially discard subhaloes at larger radii, thus bringing the radial distribution of subhaloes closer to that measured for DM.

As shown above (see right-hand panels of Fig. 1), most of the substructure mass is located at the cluster outskirts. De Lucia et al. (2004) showed that this distribution is dependent on the subhalo mass, with the most massive substructures being located at larger distances from the cluster centre with respect to less massive substructures. In particular, De Lucia et al. (2004) split their subhalo population into two subsamples by choosing a rather arbitrary mass ratio between the subhalo mass and the parent halo mass (they chose the value 0.01 for this ratio). Our simulations exhibit the same trends, but we find that this can be more or less 'significant' depending on the particular threshold adopted to split the sample. In Fig. 5, we show the radial distribution of substructures with $M_{\rm sub}/M_{200} > 0.01$ (solid lines) and $M_{\rm sub}/M_{200} < 0.001$ (dashed lines). Our trends are weaker than those found by De Lucia et al. (2004) at redshift zero, when the same division is adopted. We note, however, that these trends are dominated by the most massive substructure and are, therefore, significantly affected by low number statistics. Fig. 5 also shows that the mass segregation becomes more important at increasing redshift.

Considering that haloes of a given mass are less centrally concentrated and dynamically younger than their counterparts at later redshift, the trend found can be explained as follows: the 'younger' haloes have massive subhaloes preferentially in their outer regions because stripping has not had enough time to strip their outer material and eventually disrupt them. In more dynamically evolved clusters (those at present time), stripping has had more time to operate and to wash out any difference between the two distributions. In this picture, the balance between dynamical friction and stripping on the one hand and the accretion of new subhaloes on the other hand is such that the latter effect is dominating over the former. This is in agreement with the results shown above for the evolution of the cumulative mass function (CMF) of substructures, whose normalization increases with increasing redshift.

We stress that in Fig. 5 we are considering subhaloes of different mass at the time they are identified. As discussed in Section 1, this cannot be simply related to the mass and/or luminosity of the galaxies. So the trend shown in Fig. 5 cannot simply be related to a different spatial distribution for galaxies in different luminosity bins, as done for example in Lin, Mohr & Stanford (2004, see their fig. 8).

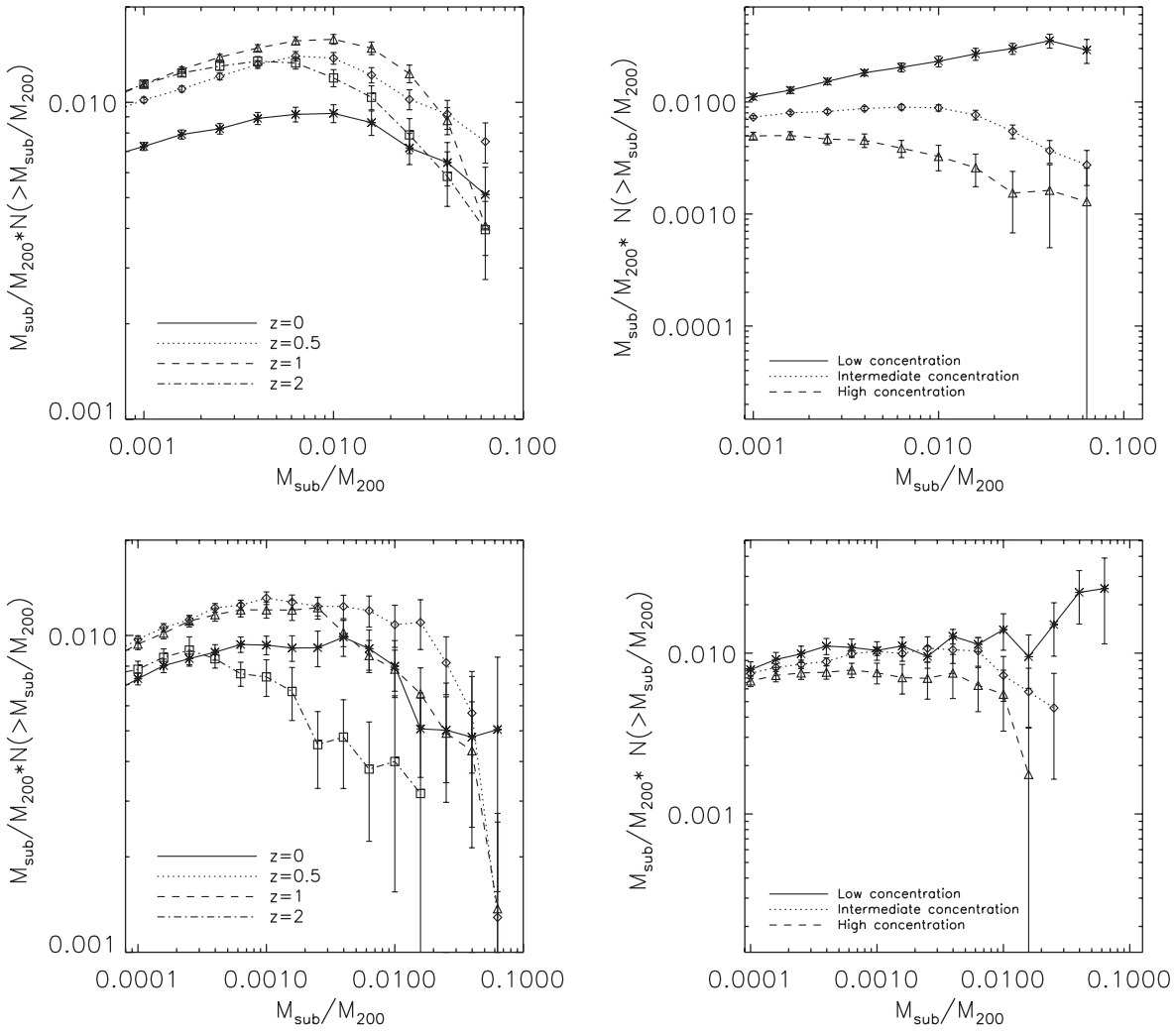

Figure 3. CMFs in units of rescaled subhalo mass, and multiplied by $M_{\rm sub}/M_{200}$ to take out the dominant mass dependence. Top and bottom panels are for haloes in the mass range (1–3) $\times\ 10^{13}\,h^{-1}\,{\rm M}_{\odot}$ and (1–5) $\times\ 10^{14}\,h^{-1}\,{\rm M}_{\odot}$, respectively. In the left-hand panel, results are shown for different redshifts (solid line for $z = 0$, dotted line for $z = 0.5$, dashed line for $z = 1$ and dot–dashed line for $z = 2$). In the right-hand panel, only haloes identified at redshift zero have been considered, and they have been split in three bins, according to their concentration. Only subhaloes with more than 100 bound particles have been used to build these functions.

4 EVOLUTION OF SUBSTRUCTURES

In this section, we study the evolution of substructures as a function of time, focusing in particular on their MAHs and merger histories. In order to obtain these information, we have constructed merger histories for all self-bound haloes in our simulations, following the method adopted in Springel et al. (2005) and the improvements described in De Lucia & Blaizot (2007).

Briefly, the merger tree is constructed by identifying a unique *descendant* for each substructure. For each subhalo, we find all haloes that contain its particles in the following snapshot, and then count the particles by giving higher weight to those that are more tightly bound to the halo under consideration. The halo that contains the largest (weighted) number of its particles is selected as descendant. Next, all the pointers to the progenitors are constructed. By default, the most massive progenitor at each node of the tree is selected as the *main progenitor*. De Lucia & Blaizot (2007) noted that this can lead to ambiguous selections when, for example, there are two subhaloes of similar mass. In order to avoid occasional failures in the merger tree construction algorithm, they modified the definition of the main progenitor by selecting the branch that accounts for most of the mass of the final system, for the longest time. We have applied this modification to our merger trees. In this section, we consider only substructures that contain at least 100 bound particles, and in a few cases, we use particular mass ranges to ease the comparison with the literature.

In this section we will also study if the accretion and merger histories of substructures depend on the environment, which we will approximate using the parent halo mass. It is worth stressing, however, that our haloes provide likely a biased sample for this analysis. In fact, excluding the most massive sample and some haloes that belong to the sample S2, all the other haloes reside in the regions surrounding the most massive haloes, which might not represent the 'typical' environment for a halo in the same mass range.

4.1 Mass accretion history

In this section, we use the merger trees constructed for our cluster sample to study the MAHs of subhaloes of different mass and

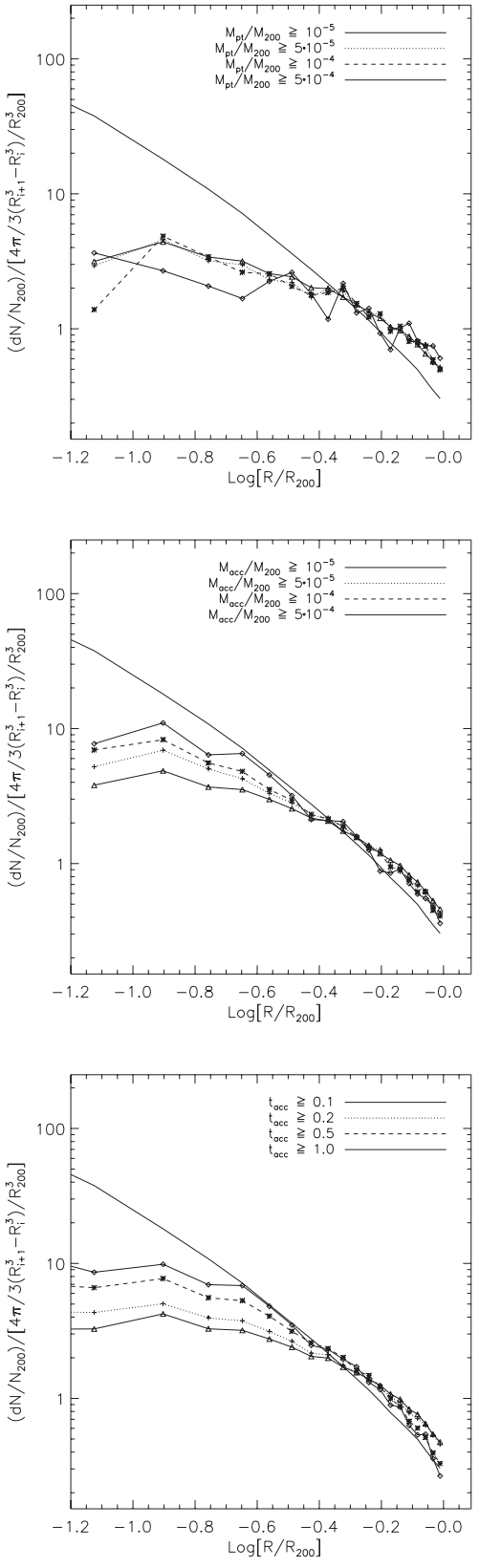

Figure 4. Radial distribution of DM substructures belonging to haloes of the sample S1. In the top panel, different lines correspond to different thresholds in the $M_{\rm sub}/M_{200}$ ratio, based on the present-day subhalo mass. In the middle panel, the subhalo mass at the time of accretion has been considered, while in the bottom panel different lines correspond to subhaloes accreted at different times.

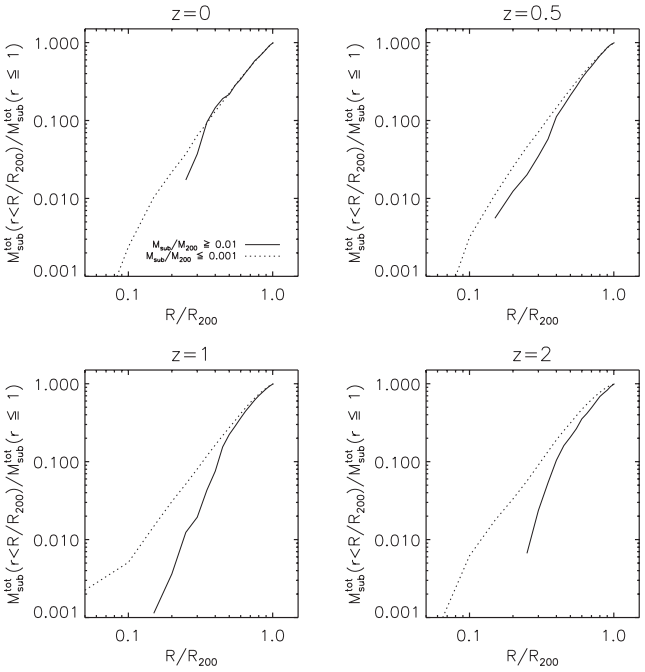

Figure 5. Cumulative radial distributions for subhaloes with $M_{\rm sub}/M_{200} > 0.01$ (solid line) and $M_{\rm sub}/M_{200} < 0.001$ (dotted line) from all samples, at different redshifts. On the y-axis, we plot the total mass in subhaloes within a given distance from the centre, normalized to the total mass in subhaloes within R_{200}, for each subhalo population.

residing in different environments. Several previous studies (De Lucia et al. 2004; Gao et al. 2004b; Warnick, Knebe & Power 2008) have pointed out that once haloes are accreted on to larger systems (i.e. they become substructures), their mass is significantly reduced by tidal stripping. The longer the substructure spends in a more massive halo, the larger is the destructive effect of tidal stripping. Previous studies have found that the efficiency of tidal stripping is largely independent of the parent halo mass (De Lucia et al. 2004; Gao et al. 2004b).

We re-address these issues using all substructures residing within the virial radius of our haloes, and with mass larger than $10^{10}\,h^{-1}\,{\rm M}_\odot$ at redshift $z = 0$ (in our simulations, these substructures contain at least 100 particles). By walking their merger trees, following the main progenitor branch, we construct the MAH for all of these subhaloes, and record the accretion time ($z_{\rm accr}$) as the last time the halo is a central halo, i.e. before it is accreted on to a larger structure and becomes a proper subhalo. Our final sample includes 39 005 haloes, which we split into two bins of different mass by using either their present-day mass or their mass at the accretion time. We end up with 33 576 haloes with mass larger than $10^{11}\,h^{-1}\,{\rm M}_\odot$ at present (25 344 when using the mass at the accretion time) and 5429 haloes with mass lower than the adopted threshold (13 661 if the accretion mass is used). In order to analyse the environmental dependence of the MAH, we consider separately subhaloes residing in our S5 and S1 samples (these correspond to our lowest and largest parent halo mass, respectively).

The top panels in Fig. 6 show the distribution of the accretion times for the two mass bins considered. Left- and right-hand panels correspond to a splitting in mass done on the basis of the present-day mass and of the mass at accretion, respectively. When considering the present-day mass (left-hand panel), the differences between the two distributions are small, with only a slightly lower fraction of more massive substructures being accreted very late, and a slightly

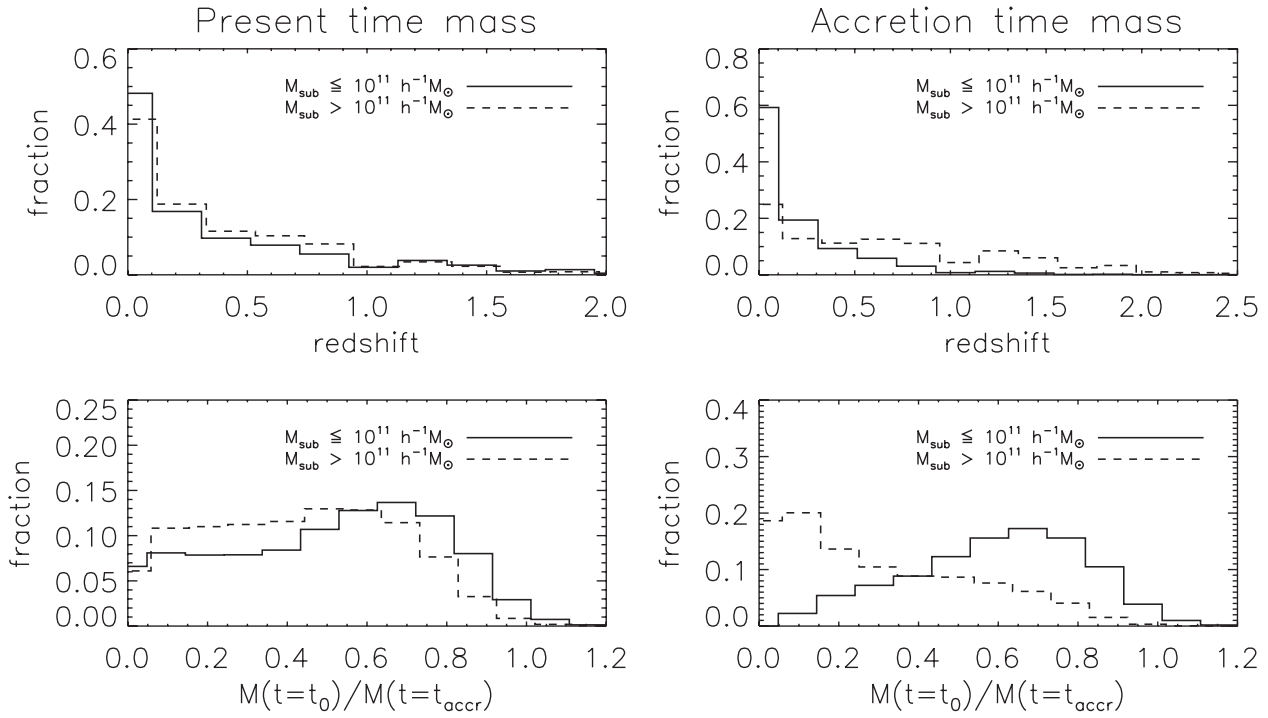

Figure 6. Left-hand panels: distribution of the accretion times (top panel) and of the fraction of mass loss since accretion (bottom panel) for subhaloes of different mass at present time (different line styles as indicated in the legend). Right-hand panels: the same distributions but for subhaloes split according to their mass at the accretion time.

larger fraction of substructures in the same mass range being accreted between $z \sim 0.1$ and 1. A larger difference between the two distribution can be seen when considering the mass at the time of accretion (right-hand panel). Substructures that are less massive at the time of accretion have been accreted on average later than their more massive counterparts. In particular, about 90 per cent of the substructures in the least massive bin considered have been accreted below redshift 0.5, while only 50 per cent of the most massive substructures have been accreted over the same redshift range. The distribution obtained for the most massive substructures is broader, extending up to redshift ∼2. This is largely a *selection effect*, due to the fact that we are only considering substructures that are still present at $z = 0$. Once accreted on to larger systems, substructures are strongly affected by tidal stripping so that, among those that were accreted at early times, only the most massive ones will still retain enough bound particles at present to enter our samples. The less massive substructures that were accreted at early times have been stripped below the resolution of our simulations and therefore do not show up in the solid histogram that is shown in the top-right panel of Fig. 6.

The bottom panels of Fig. 6 show the distribution of the ratios between present-day mass and mass at accretion for subhaloes of different present-day mass (left-hand panel) and for different mass at accretion (right-hand panel). Less massive subhaloes, which were accreted on average more recently, lose on average smaller fractions of their mass compared to more massive subhaloes for which the distribution is skewed to higher values. The difference between these distributions becomes more evident when one splits the samples according to the mass at the time of accretion, as shown in the right-hand panel. As explained above, however, this is affected by the fact that many of the least massive substructures will be stripped below the resolution of the simulation at $z = 0$. We have repeated the analysis done in Fig. 6 for subhaloes in each of the five samples used in our study, and we found there is no significant dependency on the environment.

Fig. 7 shows that, as expected, substructures accreted earlier suffered significantly more stripping than substructures that were accreted at later times. In particular, about 90 per cent of subhaloes accreted at redshift larger than 1 have been stripped by more than 80 per cent of their mass at accretion. For haloes that have been accreted at redshift lower than 1, the distribution is much broader, it

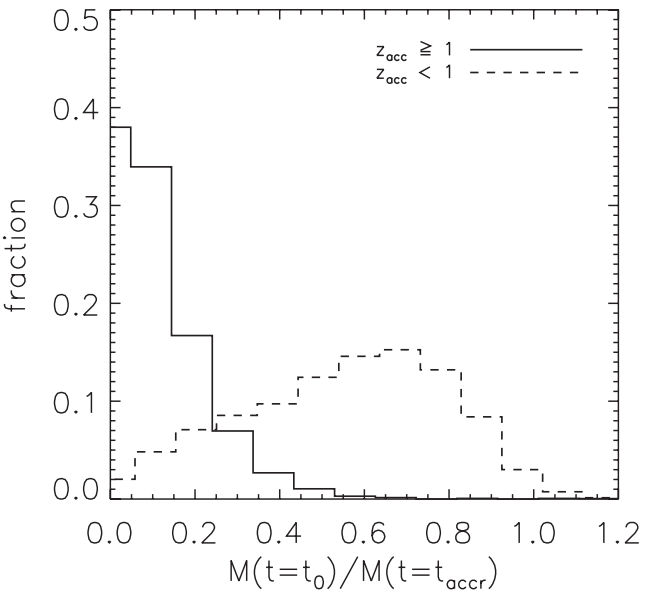

Figure 7. Distribution of mass loss (ratio between the present-day mass and the mass at accretion) for two different accretion ranges: solid line for $z_{accr} \geq 1$ and dotted line for $z_{accr} < 1$.

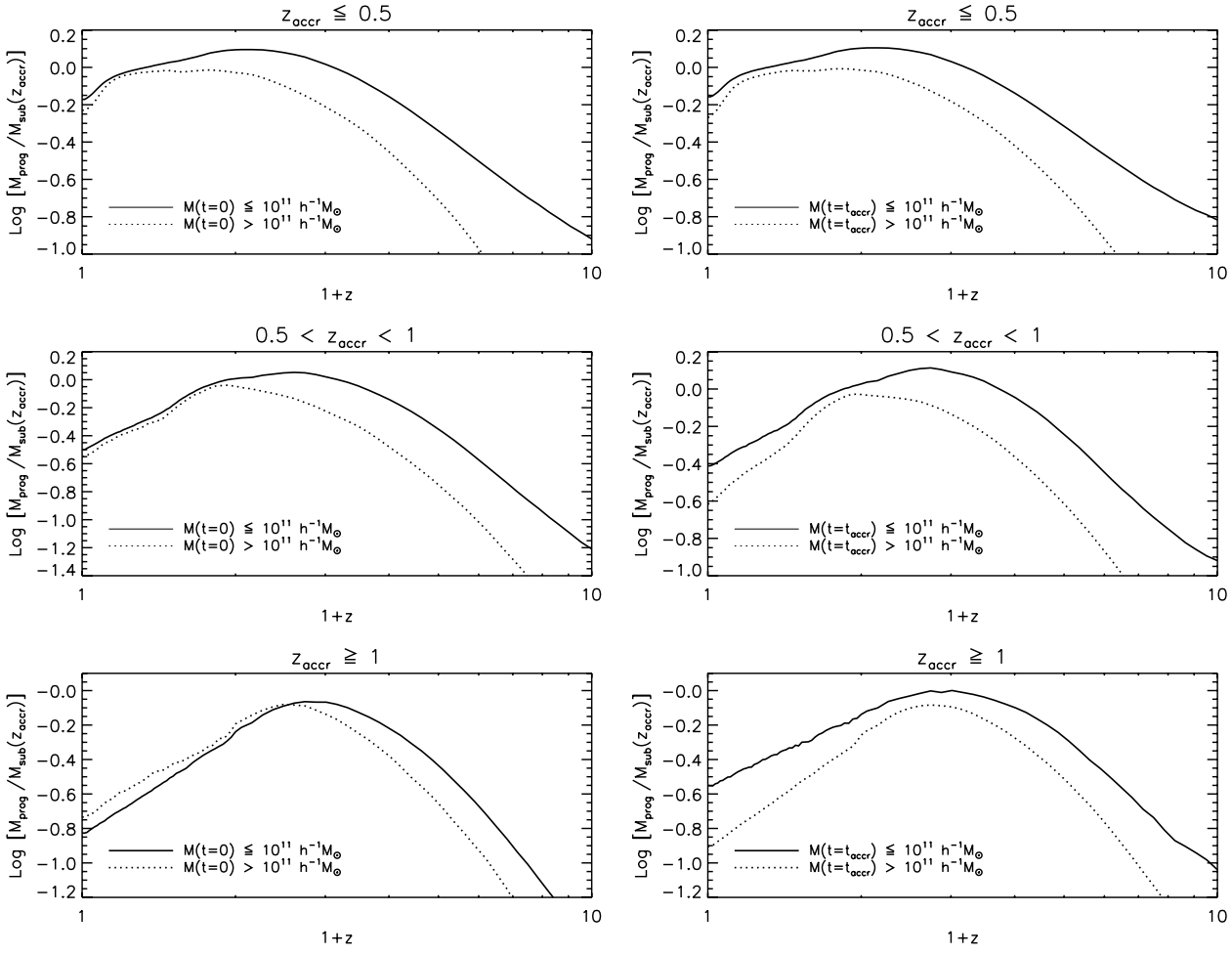

Figure 8. Average MAH for three ranges of accretion times. In the left-hand panels, substructures are split according to their present-day mass, while in the right-hand panels they are split according to their mass at the time of accretion.

peaks at ∼0.6 (i.e. about 40 per cent of the mass has been stripped for about 20 per cent of these haloes), but has a long tail to much lower values. Similarly to Fig. 6, we also tried to split this plot for different parent halo masses, without finding any significant trend with the environment.

Fig. 8 shows the MAHs of subhaloes accreted at different times. It shows results when subhaloes are split according to their present-day mass (left-hand panels) and the mass at accretion (right-hand panels). As shown in previous studies, the longer the halo is a substructure, the larger is its stripped mass. When substructures are split according to their present-day mass, the influence of tidal stripping does not appear to depend strongly on the substructure mass. In contrast, if the mass at the accretion time is considered, in a given range of accretion times, haloes that are more massive lose a larger fraction of their mass with respect to their less massive counterparts. This is due to the fact that more massive haloes sink more rapidly towards the centre because of dynamical friction, and therefore suffer a more significant stripping due to tidal interactions with the parent halo. Once again, this entails the fact that luminosity must correlate stronger with the subhalo mass computed at the time of accretion, i.e. before stripping had time to operate.

In Fig. 9 we plot the mean MAHs for subhaloes in the two mass bins considered and for two different 'environments', parametrized as the mass of the parent halo. In particular, we consider the samples S5 and S1 (i.e. the least and the most massive haloes used in our study). Dashed and long-dashed lines show the MAHs for subhaloes in the sample S5 with mass in the range $(10^{10}$–$10^{11})\,h^{-1}\,\mathrm{M}_\odot$ and larger than $10^{11}\,h^{-1}\,\mathrm{M}_\odot$, respectively. Solid and dotted lines show the MAHs for subhaloes in the same mass ranges but for the sample S1. Here we consider the present-day subhalo mass. Computing the same plot by adopting the subhalo mass at the time of accretion does not alter the results. We find that the environment does not significantly influence the MAH of substructures. In the bottom panel, the long dashed line (corresponding to substructures more massive than $10^{11}\,h^{-1}\,\mathrm{M}_\odot$ in the sample S5) is likely affected by low number statistics. In the same panel, a small difference can be seen for the less massive substructures that appear to be less stripped in the sample S5 than in S1 (compare dashed and solid lines). The difference, however, is not large, but this might be affected by the fact that our haloes all reside in the regions surrounding very massive clusters.

4.2 Merging rate

In recent years, a large body of observational evidence has been collected that demonstrates that galaxy interactions and mergers play an important role in galaxy evolution. In particular, numerical simulations have shown that major mergers between two spiral galaxies of comparable mass can completely destroy the stellar disc and leave a kinematically hot remnant with structural and kinematical

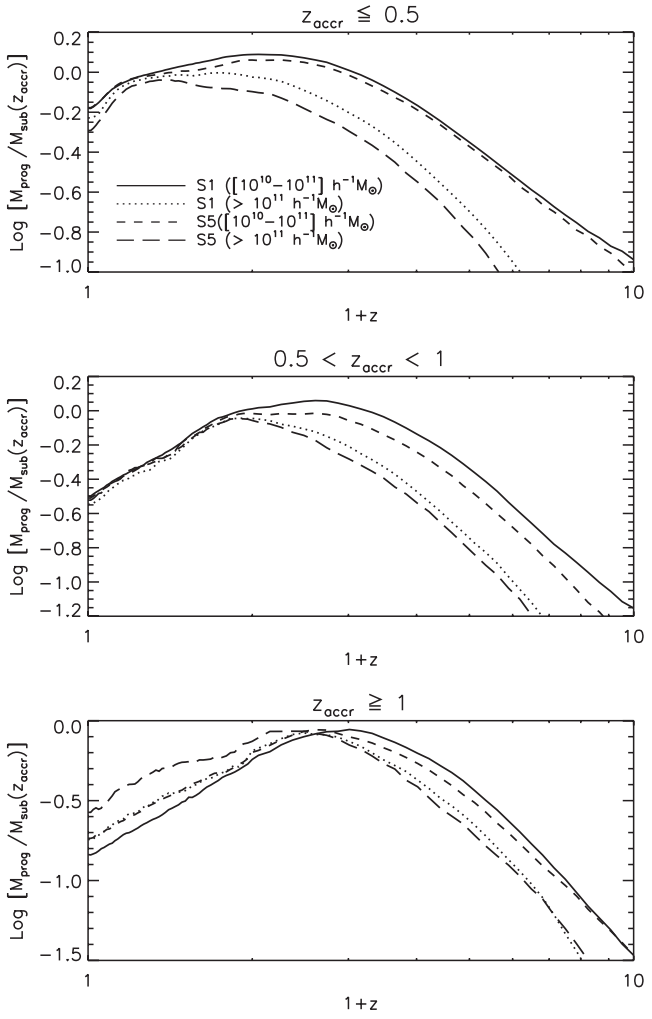

Figure 9. Average MAH for subhaloes in three different ranges of accretion time, as a function of environment. Dashed and long-dashed lines show the MAHs for subhaloes in the sample S5 with mass in the range $(10^{10}$–$10^{11})\,h^{-1}\,\mathrm{M}_{\odot}$ and larger than $10^{11}\,h^{-1}\,\mathrm{M}_{\odot}$, respectively. Solid and dotted lines show the MAH for subhaloes in the same mass ranges but for the sample S1.

properties similar to those of elliptical galaxies (Mo, van den Bosch & White 2010, and references therein). Minor mergers and rapid repeated encounters with other galaxies residing in the same halo (*harassment*; Moore et al. 1996; Moore, Lake & Katz 1998) can induce disc instabilities and/or the formation of a stellar bar, each of which affects the morphology of galaxies falling on to clusters. As galaxy mergers are driven by mergers of the parent DM haloes, it is interesting to analyse in more detail the merger statistics of DM substructures.

The MAH discussed in the previous section does not distinguish between merger events (of different mass ratios) and accretion of 'diffuse material'. In order to address this issue, and in particular to study the merger rates of DM substructures, we have taken advantage of the merger trees constructed for our samples. We have selected all subhaloes with mass larger than $10^{12}\,h^{-1}\,\mathrm{M}_{\odot}$ at redshift zero, and have followed them back in time by tracing their main progenitor branch, and recorded all merger events with other structures. In particular, we take into account only mergers with objects of mass larger than $10^{10}\,h^{-1}\,\mathrm{M}_{\odot}$, and mass ratios larger than 5:1. We note that both these values are computed at the time the halo is

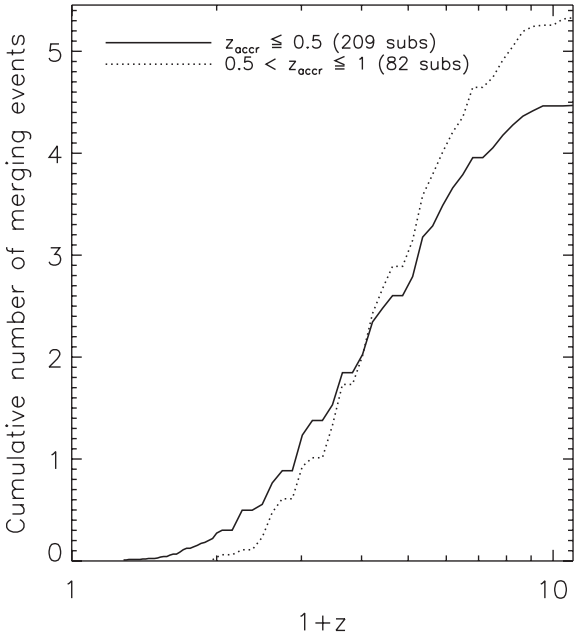

Figure 10. Mean number of major mergers as a function of redshift, for subhaloes in two different ranges of accretion time. We take into account only subhaloes with mass $M \geq 10^{12}\,h^{-1}\,\mathrm{M}_{\odot}$ at redshift $z = 0$ and merger events that include systems with mass $M \geq 10^{10}\,h^{-1}\,\mathrm{M}_{\odot}$.

for the last time central (the mass of the main progenitor at the time of accretion is considered to compute the mass ratio).

Fig. 10 shows the merging rate for all subhaloes that satisfy the above conditions. We consider in this plot only objects that experienced at least one merger event. The solid line shows the mean number of mergers for subhaloes that were accreted at $z < 0.5$, while the dotted line shows the resulting merger rate for objects accreted between the range $0.5 < z \leq 1$. The figure shows that in both cases, the slopes of the lines become shallower close to the accretion time, i.e. mergers between substructures are suppressed because of the large velocity dispersion of the parent haloes. Interestingly, haloes that were accreted earlier experience, on average, one more major merger than haloes accreted at later times.

We repeat the same analysis looking at the merging rate as a function of environment. Fig. 11 shows the cumulative number of mergers for subhaloes in our five samples. The mean number of mergers increases as a function of the parent halo mass, although subhaloes in the sample S4 experience on average fewer mergers than subhaloes in the sample S5. This is not surprising since subhaloes in the surroundings of more massive haloes have a larger probability to merge with other structures.

5 DISCUSSION AND CONCLUSIONS

We have used a large set of high-resolution simulated haloes to analyse the statistics of subhaloes in DM haloes, and their dependency as a function of the parent halo mass and physical properties of the parent halo. While some of the results discussed in this study confirm results from previous studies, it is the first time that a systematic analysis of the properties and evolution of DM substructures is carried out using a large simulation set carried out using the same cosmological parameters and simulation code. Our main results can be summarized as follows.

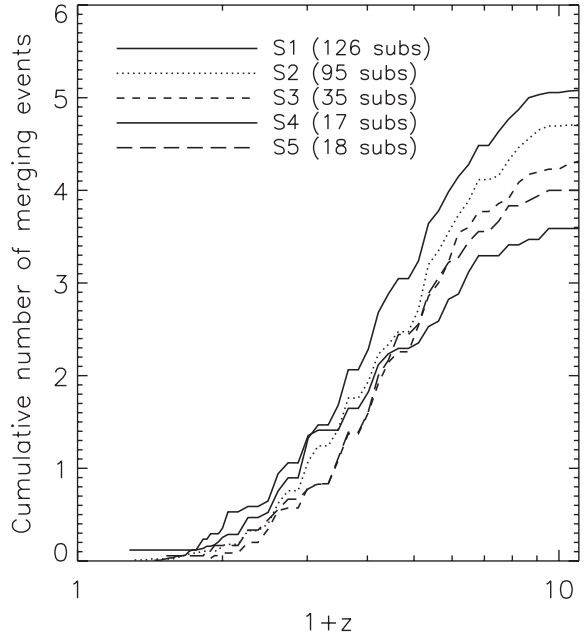

Figure 11. Mean number of major mergers as a function of redshift, for subhaloes in different environments, quantified as the mass of their parent halo. As in Fig. 10 we take into account only subhaloes with mass $M \geq 10^{12}\,h^{-1}\,\mathrm{M}_{\odot}$ at redshift $z = 0$ and merger events that include systems with mass $M \geq 10^{10}\,h^{-1}\,\mathrm{M}_{\odot}$.

(i) More massive haloes contain increasing fractions of mass in subhaloes. This does not exceed ∼10 per cent of the total mass, in agreement with previous studies. There is, however, a very large halo-to-halo scatter that can be partially explained by a range of halo physical properties, e.g. the concentration. Indeed, in more concentrated haloes substructures suffer a stronger tidal stripping so that they are characterized by lower fractions of mass in substructures.

(ii) We find that the subhalo mass function depends weakly on the parent halo mass and on redshift. This can be explained by considering that haloes of larger mass are less concentrated and dynamically younger than their less massive counterparts, and that haloes of a given mass are on average less concentrated at higher redshift. Our findings confirm results from previous studies (Gao et al. 2011) and extend them to larger halo masses.

(iii) As shown in previous work (e.g. Ghigna et al. 1998; De Lucia et al. 2004), subhaloes are antibiased with respect to the DM in the inner regions of haloes. The antibias is considerably reduced once subhaloes are selected on the basis of their mass at the time of accretion, or neglecting those that were accreted at later times. We also find that the spatial distribution of subhaloes does not depend significantly on halo mass, as suggested in previous work by De Lucia et al. (2004). The most massive substructures are located at the outskirts of haloes and this mass segregation is more important at higher redshift.

(iv) Once accreted on to larger systems, haloes are strongly affected by tidal stripping. The strength of this stripping appears to depend on the mass of the accreting substructures: those that are more massive at the time of accretion tend to be stripped by larger fractions of their initial mass.

(v) Mergers between substructures are rare events. Following the merger trees of substructures, however, we find that they have suffered in the past about four to five important (mass ratio 1:5) mergers. As expected, the number of mergers experienced depends on the environment: subhaloes in more massive systems have experienced more mergers than those of similar mass residing in less massive haloes.

DM substructures mark the sites where luminous satellites are expected to be found, so their evolution and properties do provide important information on the galaxy population that forms in hierarchical models. As discussed in previous studies, however, because of the strong tidal stripping suffered by haloes falling on to larger structures, it is not possible to simply correlate the population of subhaloes identified at a given cosmic epoch to that of the corresponding galaxies. The galaxy luminosity/stellar mass is expected to be more strongly related to the mass of the substructure at the time of *infall* and, depending on the resolution of the simulations, there might be a significant fraction of the galaxy population that cannot be traced with DM substructures because they have been stripped below the resolution limit of the simulation (the 'orphan' galaxies – see e.g. Wang et al. 2006).

Nevertheless, our results do provide indications about the properties of the galaxy populations predicted by hierarchical models. Tidal stripping is largely independent of the environment (we have parametrized this as the parent halo mass), while the accretion rates of new subhaloes increase with increasing redshift. The nearly invariance of the subhalo mass function results from the balance between these two physical processes. If the amount of DM substructures is tracing the fraction of recently infallen galaxies, the fraction of star-forming galaxies is expected to increase with increasing redshift (the 'Butcher–Oemler' effect; Butcher & Oemler 1978; Kauffmann 1995). In addition, our findings suggest that stronger mass segregation should be found with increasing redshift.

There is a large halo-to-halo scatter that can be only partially explained by a wide range of physical properties. This is expected to translate into a large scatter in e.g. the fraction of passive galaxies for haloes of the same mass, with more concentrated haloes hosting larger fraction of red/passive galaxies. Finally, there is an obvious merger bias that is expected to translate into a different morphological mix for haloes of different mass. In future work, we plan to carry out a more direct comparison with observational data at different cosmic times, by applying detailed semi-analytic model to the merger trees extracted from our simulations.

ACKNOWLEDGMENTS

We thank the anonymous referee for constructive comments that helped improving the presentation of the results. EC and GDL acknowledge financial support from the European Research Council under the European Community's Seventh Framework Programme (FP7/2007-2013)/ERC grant agreement no. 202781. This work has been supported by the PRIN-INAF 2009 grant 'Towards an Italian Network for Computational Cosmology' and by the PD51 INFN grant. Simulations have been carried out at the CINECA National Supercomputing Centre, with CPU time allocated through an ISCRA project and an agreement between CINECA and University of Trieste. We acknowledge partial support by the European Commissions FP7 Marie Curie Initial Training Network CosmoComp (PITN-GA-2009-238356). We thank A. Bonafede and K. Dolag for their help with the initial conditions of the simulations used in this study.

REFERENCES

Bonafede A., Dolag K., Stasyszyn F., Murante G., Borgani S., 2011, MNRAS, 418, 2234

Butcher H., Oemler A., Jr, 1978, ApJ, 219, 18
De Lucia G., Blaizot J., 2007, MNRAS, 375, 2
De Lucia G., Kauffmann G., Springel V., White S. D. M., Lanzoni B., Stoehr F., Tormen G., Yoshida N., 2004, MNRAS, 348, 333
Fabjan D., Borgani S., Rasia E., Bonafede A., Dolag K., Murante G., Tornatore L., 2011, MNRAS, 416, 801
Gao L., De Lucia G., White S. D. M., Jenkins A., 2004a, MNRAS, 352, L1
Gao L., White S. D. M., Jenkins A., Stoehr F., Springel V., 2004b, MNRAS, 355, 819
Gao L., Frenk C. S., Boylan-Kolchin M., Jenkins A., Springel V., White S. D. M., 2011, MNRAS, 410, 2309
Ghigna S., Moore B., Governato F., Lake G., Quinn T., Stadel J., 1998, MNRAS, 300, 146
Ghigna S., Moore B., Governato F., Lake G., Quinn T., Stadel J., 2000, ApJ, 544, 616
Ishiyama T., Fukushige T., Makino J., 2009, ApJ, 696, 2115
Kauffmann G., 1995, MNRAS, 274, 153
Klypin A., Gottlöber S., Kravtsov A. V., Khokhlov A. M., 1999, ApJ, 516, 530
Knebe A. et al., 2011, MNRAS, 415, 2293
Komatsu E., Smith K. M., Dunkley J., Bennett C. L., Gold B., Hinshaw G., 2011, ApJS, 192, 18
Lin Y.-T., Mohr J. J., Stanford S. A., 2004, ApJ, 610, 745
Mo H., van den Bosch F. C., White S., eds, 2010, Galaxy Formation and Evolution. Cambridge Univ. Press, Cambridge
Moore B., Katz N., Lake G., Dressler A., Oemler A., 1996, Nat, 379, 613
Moore B., Lake G., Katz N., 1998, ApJ, 495, 139
Moore B., Ghigna S., Governato F., Lake G., Quinn T., Stadel J., Tozzi P., 1999, ApJ, 524, L19
Nagai D., Kravtsov A. V., 2005, ApJ, 618, 557
Saro A., De Lucia G., Borgani S., Dolag K., 2010, MNRAS, 406, 729
Springel V., Yoshida N., White S. D. M., 2001, New Astron., 6, 79
Springel V. et al., 2005, Nat, 435, 629
Stoehr F., White S. D. M., Springel V., Tormen G., Yoshida N., 2003, MNRAS, 345, 1313
Tikhonov A. V., Klypin A., 2009, MNRAS, 395, 1915
Tormen G., Bouchet F. R., White S. D. M., 1997, MNRAS, 286, 865
Vale A., Ostriker J. P., 2006, MNRAS, 371, 1173
Wang L., Li C., Kauffmann G., De Lucia G., 2006, MNRAS, 371, 537
Warnick K., Knebe A., Power C., 2008, MNRAS, 385, 1859
White S. D. M., Rees M. J., 1978, MNRAS, 183, 341

This paper has been typeset from a TEX/LATEX file prepared by the author.